Post-Print of an Accepted Manuscript on the Laboratory of Turbulent Flows Website

Complete citation:

Shaban, S., Azad, M., Trivedi, J., & Ghaemi, S. (2018). Investigation of near-wall turbulence in relation to polymer rheology. Physics of Fluids, 30(12), 125111. doi: 10.1063/1.5062156

The final publication is available at https://doi.org/10.1063/1.5062156

The Accepted Manuscript begins on the next page.

Investigation of near-wall turbulence in relation to polymer rheology

Sadek Shaban,[1] Madhar Azad,[2] Japan Trivedi,[2] and Sina Ghaemi[1,a)]

[1]Department of Mechanical Engineering, University of Alberta, Edmonton, Alberta T6G 2G8, Canada

[2]Department of Civil and Environmental Engineering, University of Alberta, Edmonton, Alberta T6G 2W2, Canada

An experimental investigation was carried out to characterize the rheology of polyacrylamide solutions and its effect on the structure of a turbulent channel flow. The shear viscosity of 10 and 20 ppm solutions had similar magnitudes as water with a Newtonian behavior, while the 90 and 160 ppm solutions had shear-thinning behavior. The elasticity and relaxation time of the solutions monotonously increased with increase of polymer concentration. Pressure drop measurement at Reynold number of 20,000 showed 25, 43, 51, and 57% drag reduction for the 10, 20, 90, and 160 ppm solutions, respectively. Time-resolved planar particle image velocimetry (PIV) was used to characterize the turbulent structure. The polymers were more effective in reducing the strain-rate in the buffer layer due to the larger strain rate and stretching of the polymers. This was consistent with larger values of Weissenberg number in the buffer layer compared with the log layer. The distributions of Weissenberg number showed two distinct distributions at the low and high drag reduction regimes. The addition of the polymers to the turbulent flow was observed to balance of local strain rate and rotation. This effect was observed in the inner layer for all polymer concentrations while it was observed in the logarithmic layer only for the 90 and 160 ppm solutions. The power spectral density of turbulence kinetic energy in the buffer layer showed that the high frequency content was damped for the 10 and 20 ppm solutions while a wider frequency range was attenuated at higher polymer concentration.

[a)] ghaemi@ualberta.ca

1. Introduction

The friction between a surface and the flow can result in turbulence and loss of energy due to the subsequent viscous dissipation. It is well known that the addition of a small amount of a polymer with high molecular weight to a turbulent flow can significantly reduce this friction in internal and external flows (Ptasinski *et al.* 2001; White *et al.* 2004). The drag-reducing polymers have been successfully used in many applications such as transport of crude oil through pipelines (Burger *et al*. 1982), sewage (Sellin 1978), and firefighting systems (Fabula 1971). Although this phenomenon was reported in 1948 by Toms (Toms 1948), the mechanism of drag reduction in terms of the interaction of the polymers with the turbulence eddies is still under investigation. The previous investigations on polymer drag reduction (DR) can be divided into two categories: (a) study of turbulence statistics and structure of a polymeric flow, and (b) investigation of the behavior of polymer molecules in a turbulent flow.

One of the earliest experimental investigations on the effects of polymer on the turbulence statistics was carried out by Virk *et al.* (1967). They used a hot-film sensor and a Pitot tube to measure modification of streamwise velocity in a turbulent pipe flow of dilute polymer solution. Their work led to an empirical correlation describing the maximum drag reduction (MDR) that can be achieved in practice, known as Virk's asymptote. Warholic *et al.* (1999) investigated modification of turbulence statistics in a polymeric channel flow of a flexible polymer using laser Doppler velocimetry (LDV). They carried out the measurements for different polymer concentrations with low and high degree of DR while flow rate was kept constant. In comparison with a Newtonian flow of water at the same flow rate, streamwise Reynolds stress, normalized with friction velocity of the polymeric solution, increased at low DR ($\leq$38%) while it decreased at high DR ($\geq$55%). Decrease in wall-normal Reynolds stress and Reynolds shear stress was also observed at both low and high DR. At MDR, Reynolds shear stress is close to zero and polymer stress is finite over the cross section of the channel. Escudier *et al*. (2009) measured turbulence statistics in a fully developed turbulent channel flow of a polymeric solution while the Reynolds number based on viscosity of the polymeric solution at the wall was kept constant (i.e., variable flow rate). Their measurements for the solution of a flexible polymer demonstrated that normalized streamwise velocity increases as DR increases with increase of concentration.

The visualizations of Donohue *et al*. (1972) and Tiederman *et al*. (1985) in a channel flow showed that the spanwise spacing of low-speed streaks significantly increases and the bursting rate

decreases in a polymeric flow compared with that of the solvent alone. Mohammadtabar *et al.* (2017) investigated the turbulence structure of a rigid polymer (Xanthan Gum) in a turbulent channel flow using two-dimensional particle image velocimetry (2D-PIV). They observed that wall-normal velocity fluctuations (v) diminish at MDR while the streamwise length-scale of streamwise velocity fluctuations (u) increases. The power spectrum of u from LDV of Berman (1986), Wei & Willmarth (1992), and Warholic *et al*. (1999) showed a redistribution of energy from high frequencies to low frequencies due to addition of the polymers. Wei & Willmarth (1992) observed suppression of v spectrum over all frequencies. However, Warholic *et al*. (1999) showed a redistribution of energy from high to low wavenumber v for a similar DR. In other investigations, Warholic *et al*. (2001) used PIV in streamwise-wall-normal and streamwise-spanwise planes of a polymeric turbulent channel flow to study the wavenumber spectrum of turbulence. The spectrum of the spanwise velocity component (w) also showed redistribution of energy from high to low wavenumber structures.

The interaction between polymers and turbulence can be explained by a hypothesis proposed by Lumley (1969, 1973) based on stretching of the molecules from a coiled organization to a stretched form. This process occurs outside the viscous sublayer where fluctuating strain rate is large, and leads to local increase in effective viscosity of the solution. Lumley (1973) argued that extensional viscosity in viscous sublayer is essentially unchanged because polymer molecules are not extended in the absence of high strain rate fluctuations. Based on this hypothesis, Hinch (1977) developed an elongation model in which local extensional viscosity increases with stretching of polymer molecules. Ryskin (1987) proposed a yo-yo model that the polymer chain unravels when extensional strain rate exceeds a critical value. If extensional strain becomes weak and the flow becomes shear dominated, the polymer chain will curl back into the coiled conformation. Ryskin (1987) formulated an expression for extensional viscosity as a function of the highest extensibility of a polymer and the polymer concentration. Therefore, it is vital to perform a comprehensive measurement of extensional properties of polymer solutions for deeper insight into DR mechanism.

The majority of existing experimental studies on the extensional viscosity of polymeric solutions were carried out using capillary breakup extensional rheometry (CaBER) or filament stretching extensional rheometry (FISER) based on a uniaxial elongational flow (Plog *et al.* 2005; Clasen *et al.* 2006). Bhardwaj *et al.* (2007) conducted CaBER and FISER experiments to study the

effect of surfactant branching on the extensional rheology of wormlike micelles. Azad *et al*. (2018) explained the different recovery potential and propagation of associative polymer and hydrolyzed polyacrylamide during oil recovery applications through CaBER measurements. The FISER method is not capable of characterizing polymer solutions when the zero shear viscosity is larger than 0.5 Pa.s (Clasen *et al.* 2006; Mckinley and Sridar 2002). The CaBER method has been used to measure extensional viscosity in low viscous fluid with zero shear viscosity between 0.002 to 0.01 Pa.s (Rodd *et al*. 2005).

There has been limited information about extensional rheology of polymeric flows with DR. Gampert *et al.* (2005), Warholic *et al*. (1999), Mohammadtabar *et al*. (2017), and Escudier *et al*. (2009) only measured shear viscosity. James & Yogachandran (2006) evaluated fluid elasticity based on the breaking length of a stretched fluid bridge. They could not find a direct correlation between DR and fluid elasticity. In a more recent work, Owolabi *et al.* (2017) invetsigated the relation between DR and relaxation time. Relaxation time is defined as a time-scale to characterize the recovery of molecular configuration in viscoelastic materials after removal of an applied stress. CaBER measurements were employed to obtain the relaxation time, and developed an equation to relate DR to Weissenberg number (*Wi*). The Weissenberg number was defined as a product of relaxation time of polymer solution and mean shear rate at the wall. However, as described by Owolabi *et al.* (2017), the use of the mean wall shear rate is an approximate. The effect of extensional rheology on the distribution of fluctuating strain field of a turbulent polymeric flow, as suggested by Lumley (1973), has not been experimentally investigated yet.

The objective of this experimental investigation is to characterize the interaction between polymer molecules and turbulence by detailed measurement of the turbulent field and rheology of the polymeric solution. Measurement of mean flow, second-order turbulence statistics, and local strain-rate and rotation are carried out using time-resolved 2D-PIV in a streamwise wall-normal plane of a turbulent channel flow. A solution of polyacrylamide polymer at 10, 20, 90, and 160 ppm is used. Extensional viscosity and relaxation time of polymer solutions were obtained using CaBER system. The variation in concentration results in varying DR, with low DR for the dilute polymer solution at 10 ppm and MDR for the concentrated polymer solution at 160 ppm. The strain rate is estimated to identify regions where strong stretching or compression takes place within the flow. The investigation is extended to study the effect of polymers on the temporal scales of the

turbulent flow. The data presented in this work can also be used to evaluate models used for simulation of turbulent flow of polymeric solutions at low and high drag reduction.

2. Experimental setup

2.1 Flow loop

The experiments were carried out in a recirculating flow loop equipped with a centrifugal pump (LCC-M 50-230, GIW Industries Inc.) as shown in Figure 1.a. The flow loop had a test section with rectangular cross-section of 120 mm width (W) and 15 mm height (H). The hydraulic diameter, D_h, defined as $2WH/(W+H)$ is equal to 26.7 mm. The x-axis is parallel to the flow direction, the y-axis is normal to the bottom of the channel pointing in the upward direction, and z-axis is in the spanwise direction as shown in Figure 1.b. The walls of the test section were made from cast acrylic for optical access. The total length of the rectangular channel was 2,500 mm ($166.7H$) and the measurement location was 1600 mm ($106.7H$) downstream of the inlet of the channel inlet, ensuring a fully developed flow. The cross section gradually changed from circular to rectangular and vice versa using a three-dimensional transition sections at the entrance and exit of the channel. All experiments were carried out at a constant flow rate of 2.08 kg/s controlled by proportional integral derivative (PID) algorithm through LabVIEW software (National Instruments). This follows the works of Harder and Tiederman (1991), Warholic *et al.* (1999), Warholic *et al.* (2001), and Min *et al.* (2003), who also carried out experiments and DNS of polymer flow at the same flow rate as the Newtonian counterpart. The Reynolds number based on the full channel height H and the bulk velocity across the channel is Re_H = 20,000. The friction velocity ($u_{\tau 0}$), wall unit (λ_0), Re_τ (based on $u_{\tau 0}$ and $H/2$), and the Reynolds number based on the hydraulic diameter (Re_{Dh}) of the Newtonian flow of water are presented in Table 1.

A Coriolis flow meter (Micromotion F-series, Emerson Process Management) was used to measure mass flow rate and the density of the fluid. A K-type thermocouple probe (Omega) was used to measure fluid temperature. The fluid was maintained at a constant temperature of 25±0.2 °C using a double pipe heat exchanger. Pressure drop measurement between two pressure ports (1 meter apart) were collected using a Validyne DP-15 pressure transducer with 0.2 psi diaphragm at an accuracy of ±0.25% of the full scale. The signal from the DP-15 sensor was demodulated and amplified by a sine wave carrier demodulator (Validyne CD-15) with 1 kHz response to provide a

DC output signal. The signals were then acquired at 100 Hz frequency. The percentage of drag reduction in terms of the pressure drop (ΔP) of the polymeric and water flow is obtained using

$$DR\% = (1 - \frac{\Delta P_{polymer}}{\Delta P_{water}}) \times 100. \quad (1)$$

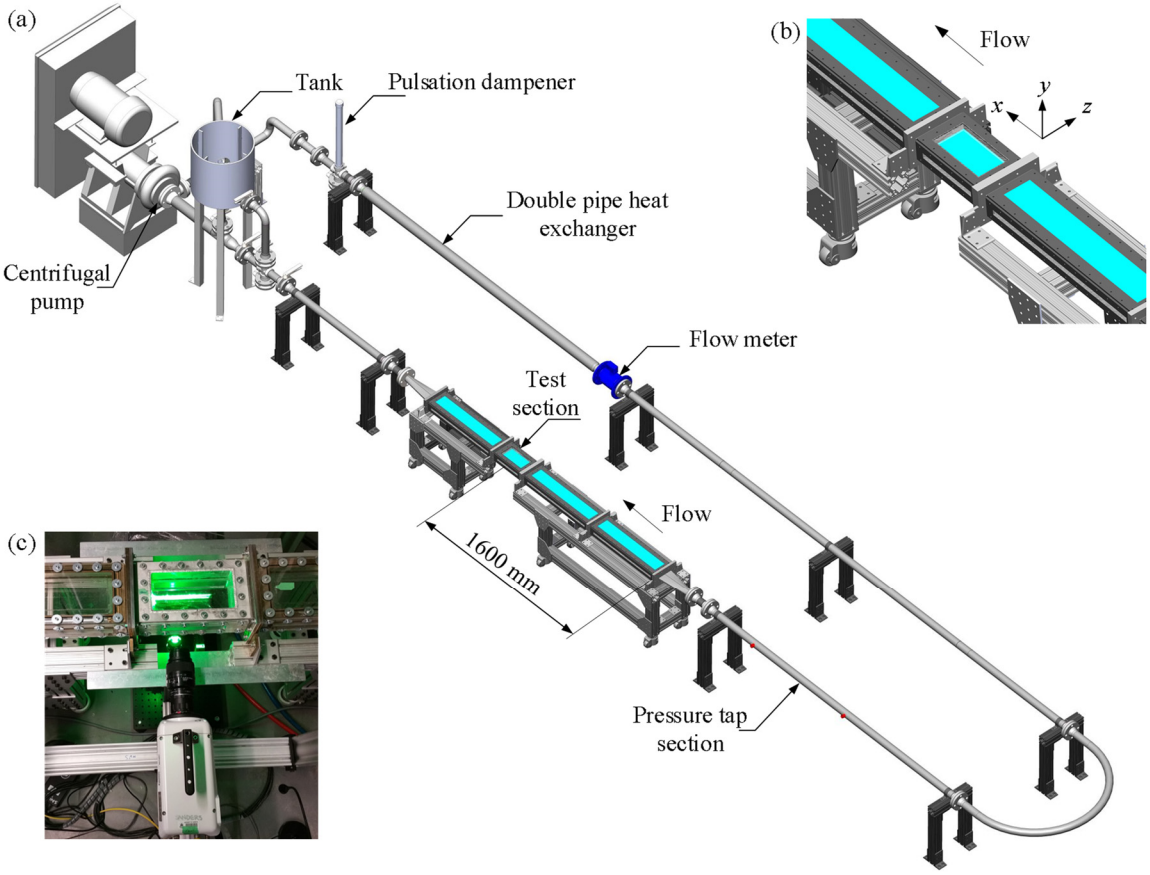

Figure 1. (a) A schematic drawing of flow loop facility, (b) test-section and the coordinate system. (c) Experimental setup of 2D-PIV showing the camera and the laser sheet illuminating an *x*-*y* plane.

Table 1. Water flow parameters at the measurement location based on planar PIV.

Parameter	Value
U_b (m/s)	1.14
Re_H	20,000
Re_{Dh}	35,100
Re_τ	507
λ_0 (μm)	14.79
$u_{\tau 0}$ (m/s)	0.0589

2.2 Polymer solution

The polymer drag reducer used in these experiments was Superfloc A-125V (Kemira Chemicals Inc.), which is an anionic polyacrylamide (APAM) with large molecular weight and medium anionic charge density. A solution of the polymer and solvent (tap water) was prepared in a mixing tank filled with 210 liters of water and equipped with a mixer (Lightnin Labmaster, L5U10F). The polymer solutions were mixed at 75 rpm for 2 hours using a three-bladed marine impeller. This mixing procedure minimizes mechanical degradation as investigated by Rowin *et al.* (2018). The dry polymer powder was added slowly to the vortex shoulder when the mixer was operated to prevent aggregation of the polymers. This procedure avoided the use of ethylene glycol, which is used to prevent polymer agglomeration. The polymer concentration was varied from 10, 20, 90, and 160 ppm to investigate dilute polymer solutions and shear thinning polymer solutions with low and high drag reduction. The amount of dry polymer required to prepare the solution was precisely weighed using a balance (Mettler Toledo, AB104-S) with a readability of 0.1 mg.

2.3 Rheological measurements

The rheology of the polymer solutions was characterized through measurement of shear and extensional viscosity. Shear viscosity was measured using a rheometer (RheolabQC, Anton Paar USA Inc.) equipped with a double gap cylinder (DG42). The double gap cylinder had a small clearance that is suitable for low viscosity fluids at high shear rate. This prevents formation of Taylor vortices and transition to turbulence (Taylor 1923). Measurements were carried out at a shear rate up to 990 s^{-1} at constant temperature of 25˚C.

In this study, the extensional rheological behavior of superfloc A125V was evaluated using a capillary break-up extensional rheometer (Haake CaBER, Thermo Scientific). A small sample of each polymer solution was placed carefully between two circular plates with 6 mm diameter using a syringe. The movable plate at the top was rapidly separated from the stationary bottom plate. The movement causes formation of a filament by imposing an instantaneous level of extensional strain on the fluid sample. A strike time of 50 milliseconds (ms) was applied for the separation of plates. The stretched fluid was squeezed together by the capillary force. The midpoint diameter of the thinning fluid filament (D_{mid}) was monitored with a laser micrometer as a function of time (t). The balance between the driving capillary force and the resistive viscous and elastic force governs the filament drainage.

The relaxation time of the polymeric solution (τ_{ext}) was obtained using the upper-convected Maxwell (UCM) model (Joseph 1990, Kim *et al*. 2010) following

$$D_{mid}(t) = D_0 \left(\frac{G\, D_0}{4\,\sigma}\right)^{\frac{1}{3}} e^{\left(\frac{-t}{3\tau_{ext}}\right)}, \qquad (2)$$

where G is the elastic modulus of the filament, D_0 is the initial diameter of the filament. The surface tension of polymer solution (σ) was assumed to be the same as water and equal to 73×10^{-3} N/m. The experimental work of Miller *et al*. (2009) showed that even at high polymer concentration (10,000 ppm, polyacrylamide) surface tension does not change significantly and is still about 72×10^{-3} N/m. Both G and τ_{ext} were obtained by fitting this equation on the linear section of a semi-logarithmic plot of diameter D_{mid} (logarithmic axis) versus time (linear axis). The linear section of the semi-logarithmic plot represents the elastic region during the filament drainage with exponential decline of fluid diameter. A viscoelastic material sustains a deformed state for a certain time after removal of the stress, which is characterized using a relaxation time. In polymer solutions with flexible molecular structure, the relaxation time refers to the time scale that quantifies the tendency of the molecules to coil to an initial state after being stretched (Stelter & Brenn 2002).

The evolution of the midpoint diameter is governed by the balance between forces on the filament as

$$3\eta_S\left(-\frac{2}{D_{mid}}\,\frac{d\,D_{mid}}{dt}\right) = \frac{F_Z}{\pi\,(D_{mid}/2)^2} - [\tau_{zz} - \tau_{rr}] - \frac{\sigma}{(D_{mid}/2)}\,, \qquad (3)$$

where F_z is the tensile force acting on the column ends and η_s is solvent viscosity (Yarin 1993; Renardy 1995; Reichel *et al*. 2016). The term on the left-hand side of equation (3) represents the viscous stress. The τ_{zz} and τ_{rr} terms indicate normal stress components in the axial and radial direction, respectively, representing the non-Newtonian elastic stresses. The last term on the right-hand side expresses capillary pressure force.

The evolution of the midpoint diameter of fluid samples with time is driven by the capillary pressure and resisted by the elastic stress and viscous stress (Anna & McKinley 2001; McKinley 2005; Kim *et al*. 2010). When the top plate reaches the final height, the tensile force becomes zero (Anna & McKinley 2001), therefore, equation (3) is reduced to

$$3\eta_S\left(-\frac{2}{D_{mid}}\frac{d\,D_{mid}}{dt}\right)+[\tau_{zz}-\tau_{rr}]=\frac{2\sigma}{(D_{mid})}\,. \tag{4}$$

The extensional strain (ε) is defined as Hencky strain following (Schümmer & Tebel 1983)

$$\varepsilon(t)=2\,\ln\left(\frac{D_0}{D_{mid}(t)}\right). \tag{5}$$

The strain rate is defined as (Schümmer & Tebel 1983)

$$\dot{\varepsilon}(t)=-\frac{2}{D_{mid}(t)}\left(\frac{d\,D_{mid}(t)}{dt}\right). \tag{6}$$

The extensional viscosity (η_{ext}) is defined following

$$\eta_{ext}=-\frac{(2z\text{-}1)\sigma}{\frac{dD_{mid}}{dt}}, \tag{7}$$

as detailed in the previous studies by Anna & Mckinley (2001) and Kim *et al*. (2010). In this equation, z is a correction factor for axial variation and its value is 0.7127 in the CaBER experiment (McKinley & Tripathi 2000). Three independent measurements, using separately prepared polymer solutions, were carried out for each polymer solution to verify the repeatability and estimate the uncertainity.

2.4 Planar particle image velocimetry (PIV)

Planar PIV measurements were carried out to measure the velocity field in an *x-y* plane at the mid-span of the channel as shown in Figure 1.c. A high-speed CMOS camera (Phantom v611, Vision Research) with sensor size of 1280 × 800 pix was applied. Each pixel of the CMOS sensor is 20 × 20 μm^2 with 12-bit resolution. The camera was equipped with a Nikon lens with focal

length of f = 105 mm, at aperture setting of f/8. For the illumination of tracer particles, a dual-cavity Nd:YLF Laser (DM20- 527 DH, Photonics Industries Inc.) was used with output of 20 mJ per pulse at 1 kHz, and maximum repetition rate of 10 kHz per cavity. The laser beam was shaped into a sheet with thickness of ~1 mm using a combination of cylindrical and spherical lenses. Silver-coated glass spheres (SG02S40, Potters Industries Conduct-O-Fil®) were used as flow tracers with density of 3.6 g/cm^3 and diameter of 2 μm. The digital resolution of the imaging system is 71.4 pixel/mm at magnification of M = 1.42. The field of view (FOV) is 12.5 mm × 5.4 mm in the streamwise and wall-normal directions, respectively. The depth-of-focus (DOF) is estimated about 1.8 mm. The PIV images were captured as single-frame images at 16 kHz with a pulse separation of Δt = 62.5 μs. The synchronization of laser and camera was accomplished by a programmable timing unit (PTU X, LaVision GmbH), which was controlled by DaVis 8.3 (LaVision GmbH) software.

Six datasets of 16,000 time-resolved singe-frame images was acquired for every polymer concentration and the baseline case of water. In order to increase the signal to noise ratio, the minimum intensity of the ensemble was subtracted from the individual images, then each image was normalizing using the ensemble average. The instantaneous velocity fields were obtained using a sliding-correlation applied to two successive pairs of images with time step of 2Δt (125 μs) to reduce the cross-correlation noise (Meinhart *et al*. 2000; Ghaemi *et al*. 2012). The sliding-correlation was performed with final interrogation window size of 16×16 pix (224×224 μm^2) with 75% overlap. The vector fields for the mean velocity profile were obtained from the ensemble of correlation applied to all the images (Meinhart *et al*. 2000) with final window size of 6×6 pix (84×84 μm^2) with 75% overlap and 4:1 aspect ratio in the streamwise direction. The processing of all PIV data sets was conducted in Davis 8.3 (LaVision, GmbH) and the parameters are summarized in Table 2.

Table 2. Specification of the planar PIV system. The dimensions with superscript + are normalized using wall unit λ_0 = 14.79 μm of water flow.

Data set	16,000	
Magnification	1.42	
Digital resolution	71.4 pix/mm	
Acquisition frequency	16,000 Hz	
Measurement field (Δx, Δy)	892×385 pix	
	12.5×5.4 mm^2	
	$845.2^+ \times 365.1^+$	
Velocity evaluation	Sliding-correlation	Ensemble of correlation
Interrogation window (Δx, Δy)	16×16 pix	6×6 pix
	224×224 μm^2	84×84 μm^2
	$15.2^+ \times 15.2^+$	$5.7^+ \times 5.7^+$

3. Results and discussion

In this section, the interaction between polymers and turbulence in near the wall region, which is manifested as reduced drag, is investigated in dilute and shear thinning polymer solutions. The rheological properties of drag-reducing polymer are characterized. The turbulence data obtained from time-resolved 2D-PIV in *x*-*y* plane is used to study the turbulence structure including the strain field of the polymeric channel flow.

3.1 Characterization of non-Newtonian fluid

The shear viscosity versus shear rate for polymer solutions and water are compared in Figure 2. The viscosity of dilute polymer solutions (10 and 20 ppm) is slightly larger than the viscosity of water, which shows Newtonian behavior. As polymer concentration increases, the solution viscosity increases and non-Newtonian behavior appears. The polymer solutions of 90 and 160 ppm exhibit shear-thinning behavior, in which viscosity decreases with increase of shear rate.

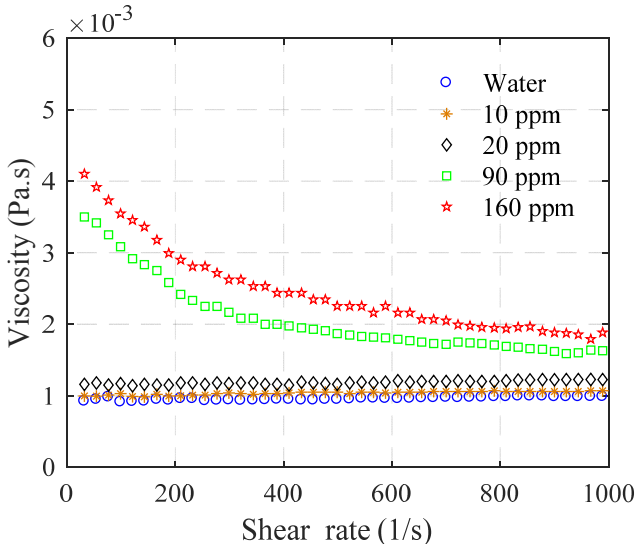

Figure 2. Shear viscosity as a function of shear rate for water and the four polymer solutions showing Newtonian and shear-thinning behavior.

Figure 3 shows the effect of polymer concentration on filament diameter as a function of time, measured using the CaBER. The time reference of $t = 0$ represents when the top plate reaches the final height and stops moving. The error bars show maximum variation based on repeated measurements. The results show that dilute polymer solutions of 10 and 20 ppm break up at a diameter of 0.082 and 0.057 mm, respectively. There is an increase in resistance to capillary force at 20 ppm compared with 10 ppm. The filament diameter of the concentrated polymer solutions of 90 and 160 ppm decreases to 0.031 and 0.016 mm before the breakup, respectively. The dilute polymer solutions undergo a faster filament breakup than concentrated polymer solutions due to their lower elasticity. The larger error bars for the low concertation solutions is mainly associated with the faster filament break up, which also reduces the number of data points. It is also observed that the error bars become larger before the filament breaks up.

The relaxation time is determined using the UCM model following equation 2, and the results are presented in Table 3. It is observed that relaxation time increases with increasing polymer concentration. Therefore, concentrated polymer solutions have higher resistance and slower response to capillary force compared with the dilute polymer solutions. For instance, the relaxation time for 160 ppm is 8.8 times larger than that of 10 ppm, implying that a longer time is required to respond to extensional strain. The polymer solutions that have higher relaxation time have more

elasticity (Marshal and Metzener 1967). Delshad *et al*. (2008) used the relaxation time to represent the elasticity of polymers in a viscoelastic model.

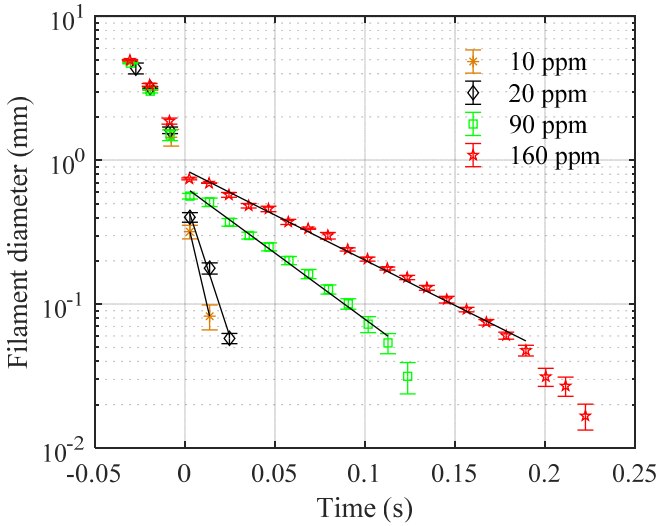

Figure 3. A semi-logarithmic plot of filament diameter as a function of time for four different polymer concentrations. The line represents fitted values using UCM model, equation (2). The error bars represent minimum and maximum filament diameter based on three independent measurements.

The effect of polymer concentration on the extensional viscosity as a function of Hencky strain is presented in Figure 4. The time derivative $D_{mid}(t)$ in equation (7) is obtained from the linear section of data in Figure 3. The increase of extensional viscosity (η_{ext}) with ε shows strain hardening behavior. The solutions with lower concentration of 10 and 20 ppm show this behavior at slightly smaller values of ε. The 90 and 160 ppm show strain hardening at an order of magnitude larger η_{ext} than the dilute solutions. The maximum extensional viscosity for polymeric solutions is also listed in Table 3.

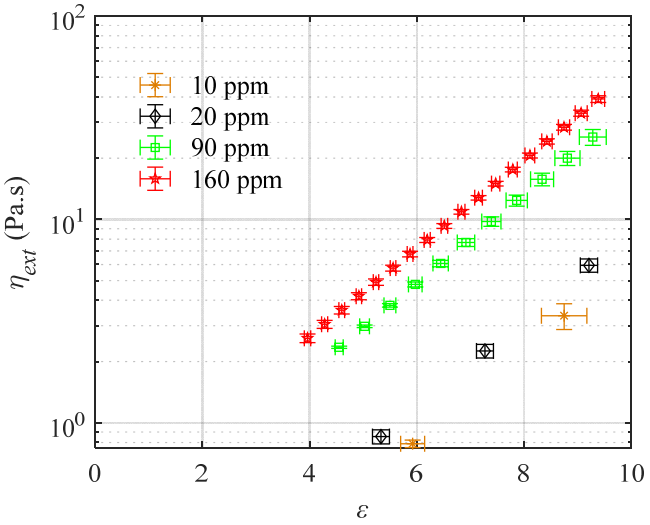

Figure 4. Extensional viscosity of different polymer solutions as a function of Hencky strain. The error bars represent minimum and maximum of values from three independent measurements.

A semi-logarithmic plot of extensional viscosity as a function of strain rate for four different polymer concentrations are presented in Figure 5. It is observed that filament drainage for concentrated polymer solutions occurs at a low strain rate ($\dot{\varepsilon}$ < 50 1/s) and high extensional viscosity ($\eta_{ext} \geq 2$). For dilute polymer solution, the filament drainage occurs at a higher strain rate ($\dot{\varepsilon}$ > 150 1/s) and lower extensional viscosity, while the filament breaks quickly. The data is used to also estimate the Deborah number (*De*), defined as the product of relaxation time and strain rate (Kim *et al.* 2010). Deborah number of the solutions is shown in Figure 6 and characterizes the strength of the extensional flow (Rothstein 2003). When *De* approaches zero, the fluid behaves as a purely viscous Newtonian fluid. When *De* becomes larger, the elastic behavior of the fluid becomes pronounced (Christanti and Walker 2001; Chhabra 2010). The lowest *De* before the breakup point is observed for the 10 ppm solution, implying the polymer has small elasticity. As polymer concentration increases, the maximum Deborah number increases, and the polymer solution becomes more elastic. The maximum *De* of 10, 20, 90, and 160 ppm solutions is 0.66, 0.70, 0.76 and 0.78, respectively.

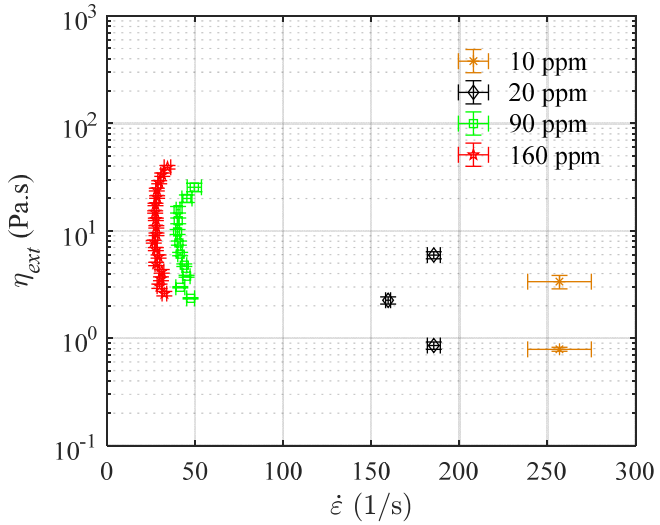

Figure 5. A semi-logarithmic plot of extensional viscosity as a function of strain rate.

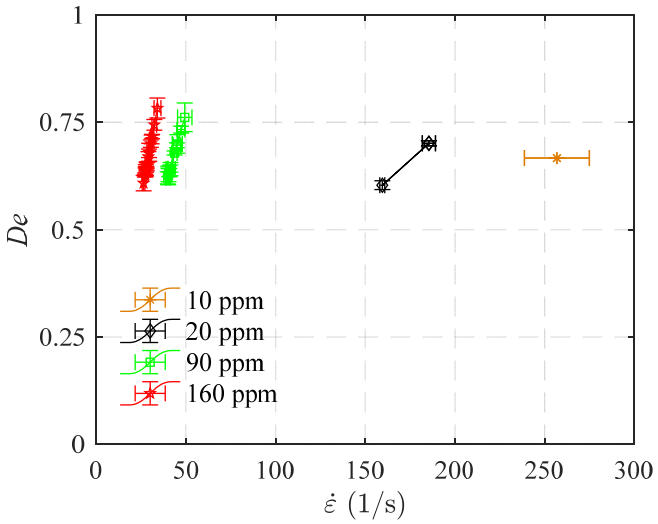

Figure 6. Effect of polymer concentration on Deborah number.

3.2 Turbulent flow field

In this section, statistical characterization of the turbulent channel flow of APAM at different concentrations is compared with the Newtonian flow of water. The percentage of DR at each concentration is obtained from pressure drop measurement as presented in Table 3. As it is expected, the results show that DR increases with increase of polymer concentration. The DR of 20 ppm is about twice the DR of 10 ppm, while their shear viscosity is similar. The difference is associated with extensional viscosity and larger relaxation time (42.30%) of the 20 ppm solution.

The change in DR is only 6% when concentration is increased from 90 to 160 ppm. Therefore, the solution at 160 ppm has approached MDR. The effect of change in rheology of the solution on turbulent statistics is scrutinized here.

3.2.1 Mean velocity profile

The mean streamwise velocity $<U>$ normalized by the bulk velocity U_b in the near-wall region for the polymer solutions and water is presented in Figure 7.a. The velocity profile of dilute polymer solutions with 10 and 20 ppm is closer to the velocity profile of water. For the shear thinning solutions with 90 ppm and 160 ppm polymer concentration, the velocity profiles are between the profiles of turbulent and laminar flow of water. In general, the velocity of the polymeric flows is smaller than that of water in the near wall region, while it is larger further away from the wall to maintain the same mass flow rate across the channel. The velocity gradient at the wall $d<U>/dy|_w$ is calculated using a linear regression based on the data within $y/H < 0.005$ and presented in Table 3. In general, $d<U>/dy|_w$ reduces with increase of polymer concentration. The drag reduction can also be calculated as $\mu_w d<U>/dy|_w$, where μ_w is shear viscosity of polymer solution based on the strain rate at the wall (i.e., $d<U>/dy|_w$) and estimated using Figure 2. The obtained value is indicated as DR* and presented in Table 3. The results are within a few percentage of the DR based on pressure drop measurement.

A semi-logarithmic plot of the normalized mean streamwise velocity profile ($U^+ = <U>/u_\tau$) versus wall-normal distance ($y^+ = y/\lambda$) is presented in Figure 7.b, where u_τ and λ are the corresponding friction velocity and wall unit, respectively. The shear viscosity (μ_w) and velocity gradient at the wall are used to obtain the inner scaling. The semi-logarithmic profile for water is in agreement with law of the wall ($u^+ = y^+$) and the von-Kármán log-law ($U^+ = 1/\kappa \, ln \, y^+ + B$) with $\kappa = 0.389$ and $B = 5.5$, confirming a fully developed turbulent channel flow. The profiles of polymeric flows and water overlap in the viscous sublayer ($y^+ < 5$). However, the viscous sublayer in polymeric flows extends beyond $y^+ = 5$ as also observed by Escudier *et al.* (2009). The log-region shifts upward and the buffer layer thickens with increase of polymer concentration, in agreement with Warholic *et al.* (1999). It is also noted that the slope of the logarithmic layer remains parallel to that of the Newtonian flow in dilute polymer flows, while the slope increases for the 90 and 160 ppm solutions. Ptasinski *et al.* (2001) and Mohammadtabar *et al.* (2017) also observed a similar trend. The upward shift of the log-layer implies that the balance between the turbulent energy production and the viscous dissipation occurs farther away from the wall (Choi

1989). The profile of the 160 ppm solution reaches the MDR asymptote, determined empirically by Virk *et al.* (1970) as $U^+ = 11.7\ ln\ y^+ - 17$.

The DR is also evaluated based on *Wi,* defined as $\tau_{ext}\dot{\gamma}$, where $\dot{\gamma}$ is assumed to be $d<U>/dy|_w$ following Owolabi *et al.* (2017). The results in Table 3 shows that DR increases with *Wi*, except at 20 ppm. The *Wi* of the 20 ppm solution is also slightly smaller than *Wi* of the 10 ppm solution, although the DR of 20 ppm is about twice the DR of 10 ppm. The increase of DR with *Wi* was observed by Owolabi *et al.* (2017) for 150, 250, and 350 ppm of FloPAM solution and 250 ppm of Separan solution while *Re* number was varied (i.e. $d<U>/dy|_w$ varied). Although the trend is similar, DR magnitudes of the current study for 10 and 20 ppm are 2.7 and 1.5 times smaller than those predicted using DR versus *Wi* correlation suggested by Owolabi *et al.* (2017). The variation is associated with the different polymer type used in these two studies and the smaller relaxation time of the dilute 10 and 20 ppm solutions.

Table 3. Drag reduction, rheological properties, and flow parameters of the polymer solutions. DR is based on pressure drop measurement and DR*% is calculated based on τ_w from PIV measurement.

	DR %	DR* %	*Wi*	τ_{ext} (s)	Maximum η_{ext} (Pa.s)	u_τ (m/s)	μ_w (Pa.s)	$d<U>/dy|_w$ (1/s)	λ (μm)
10 ppm	25	23	6.96	0.0026	3.36	0.052	$1e^{-3}$	2680	19.29
20 ppm	43	42	6.24	0.0037	5.94	0.0452	$1.2e^{-3}$	1687	26.63
90 ppm	51	54	15.60	0.0155	25.40	0.0392	$1.6e^{-3}$	1007	40.94
160 ppm	57	60	15.70	0.0230	39.07	0.0374	$2.05e^{-3}$	683	54.98

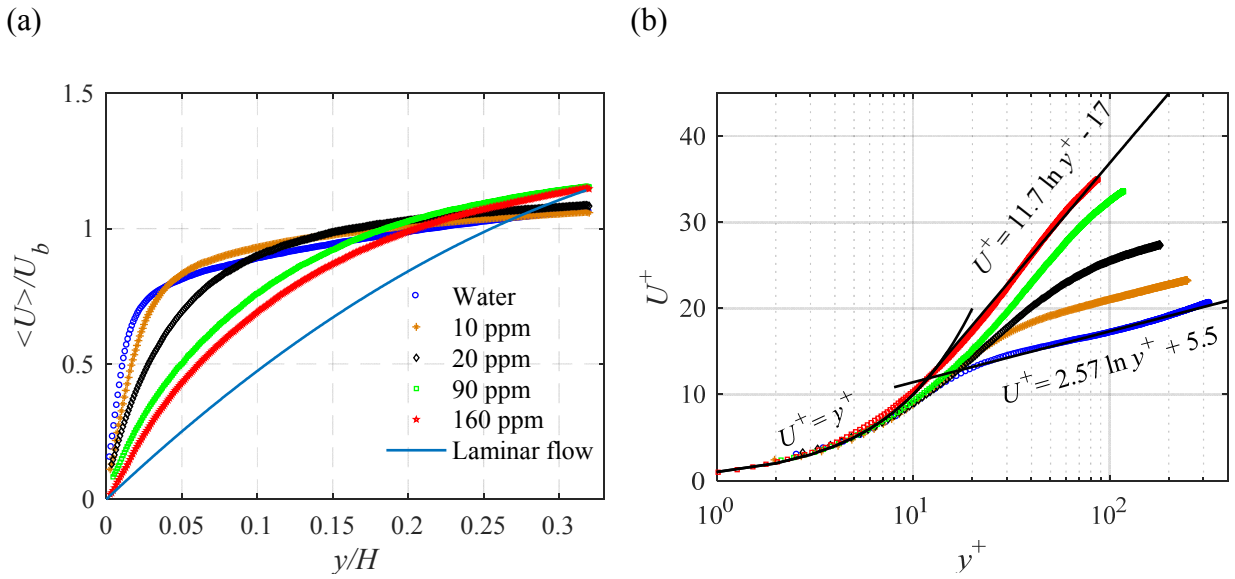

Figure 7. The effect of polymer concentration on the (a) mean streamwise velocity normalized by the bulk velocity as a function of the wall-normal location, and (b) the semi-logarithmic profile of mean streamwise velocity. The law of the wall ($U^+ = y^+$), log-law of Newtonian flows ($U^+ = 2.57 \ln y^+ + 5.5$), and Virk's asymptote ($U^+ = 11.7 \ln y^+ - 17$) for MDR are also shown.

3.2.2 Reynolds stresses

The profiles of Reynolds stress normalized by the inner scaling of water ($u_{\tau 0}$), instead of u_τ of the polymer solution, are shown in Figure 8. The applied normalization avoids variation of Reynolds stresses due to change in friction velocity. The erroneous data points in the vicinity of the wall ($y_0^+ < 16$) due to PIV bias error have been removed to avoid any ambiguity. The PIV biased error in the first few near-wall vectors result from the mirrored particle images, signal truncation, and the glare of the laser light in the near-wall interrogation windows (Theunissen *et al*., 2008). The results obtained from measurement in water at $Re_\tau = 507$ agree with DNS of fully developed Newtonian channel flow by Lee & Moser (2015) at $Re_\tau = 544$. The peak of streamwise Reynolds stress, $\langle u^2 \rangle / u^2_{\tau 0}$, decreases and shifts towards the center of the channel with increase of polymer concentration. This is in agreement with Warholic *et al* (1999) for low and high DR regimes when a similar normalization is applied. The trend also agrees with increase in thickness of the viscous and buffer layers as observed in the semi-log plot of Figure 7.b.

The profiles of wall-normal Reynolds stress, $\langle v^2 \rangle / u^2_{\tau 0}$, are presented in Figure 8.b. Relative agreement with DNS results is observed for water. The $\langle v^2 \rangle$ peak at 10 ppm reduces by 52% and the peak location is shifted away from the wall to $y_0^+ = 130$ relative to that of water. The reduction of $\langle v^2 \rangle$ profiles continues as polymer concentration increases similar to observations of Warholic

et al. (1999) and Escudier *et al.* (2009). The normalized profiles of Reynolds shear stress $\langle uv \rangle / u^2_{\tau 0}$ in Figure 8.c reduces with increase of concentration. The location of the peak moves away from the wall with increase of polymer concentration up to 20 ppm. The value of $\langle uv \rangle$ is negligible at 90 and 160 ppm, which are close to MDR. This is consistent with previous experimental observations of Warholic *et al*. (1999, 2001).

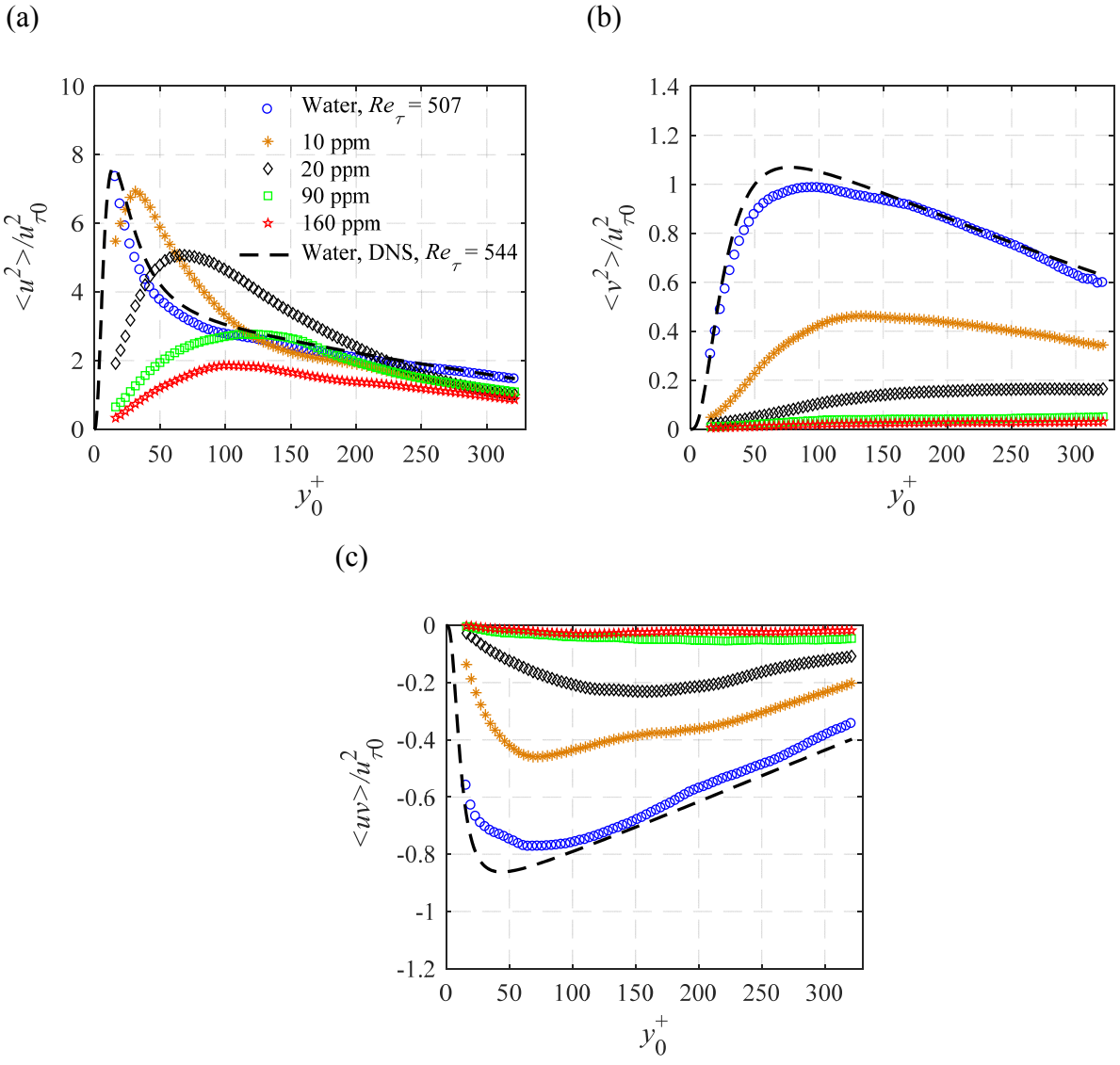

Figure 8. The effect of polymer concentration on (a) streamwise, (b) wall-normal, and (c) shear Reynolds stress normalized by the friction velocity of water ($u_{\tau 0}$).

3.2.3 Quadrants of velocity fluctuations

The contribution of ejection and sweep motions to turbulence production is investigated using conditional averaging of Reynolds stress, following Willmarth and Lu (1972). A conditional averaging of $<uv>$ based on the four quadrant of v versus u plot is carried out, and the results are presented in Figure 9 for water and the polymer solutions. The turbulent motions of the second and fourth quadrant increase the turbulence kinetic energy, while the motions of the first and third quadrant reduce the turbulence production.

In figure 9.a, a significant reduction of $<uv>$ averaged based on motions in first quadrant, $<uv_{Q1}>$, is observed for high polymer concentrations. Figure 9.b shows that contribution of ejection motions to turbulence production, $<uv_{Q2}>$, decreases with increase of polymer concentration. The location of the peak moves away from the wall with increasing polymer concentration in dilute polymeric flows, whereas the peak almost vanishes for 90 and 160 ppm. A similar trend is observed for $<uv_{Q3}>$ and $<uv_{Q4}>$ in Figure 9.c and d. In general, $<uv_{Q2}>$ events dominate turbulence production away from the wall, while $<uv_{Q4}>$ events dominate in the vicinity of the wall. The profiles of $<uv_{Q4}>$ for polymeric flows attenuate and the intensity of sweep motions decreases with increase of polymer concentration.

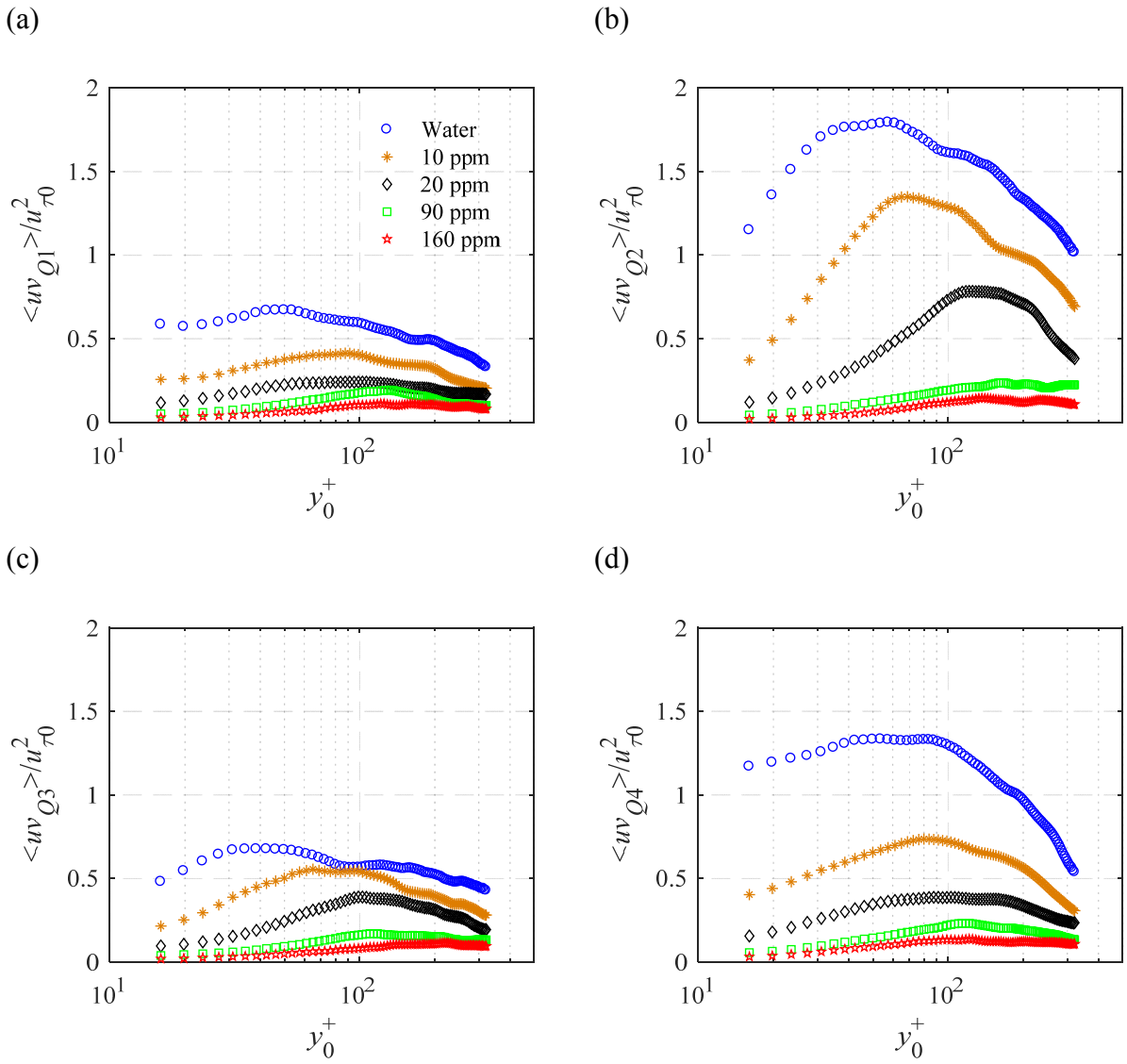

Figure 9. Evaluation of the conditional averages <*uv*> based on four quadrants of turbulent velocity fluctuations: (a) uv_{Q1}, (b) uv_{Q2}, (c) uv_{Q3}, and (d) uv_{Q4}.

3.3 Velocity gradient tensor

The spatial distribution of velocity gradient in a turbulent flow plays a significant role in polymer DR by interacting and stretching the polymers. The velocity gradient field consists of rotational (asymmetric) and strain-rate (symmetric) components. In a pure rotational flow, a polymer chain rotates without any deformation, while in a pure strain field (i.e., elongational flow) a polymer can significantly stretch (Smith *et al*., 1999). However, in a turbulent flow rotation and strain-rate occur simultaneously. This may not result in a significant stretching of the polymers as the rotation (tumbling) relaxes the stretching process (Lumley, 1969; Doyle *et al.,* 1997).

Therefore, deformation of the polymer molecules depends on the relative magnitude of strain-rate and rotation in the turbulent flow, as we investigate in this section.

3.3.1 Normal strain-rate

The effect of polymer concentration on two normal components of the strain rate tensor, which are available from planar PIV, is investigated here. The streamwise strain-rate (S_{11}) is calculated following

$$S_{11}=\frac{\partial U}{\partial x} \quad , \tag{8}$$

and the wall-normal strain-rate is obtained from

$$S_{22}=\frac{\partial V}{\partial y} \quad . \tag{9}$$

The probability density function (PDF) of S_{11} at two different wall-normal locations of $y_0^+ = 24$ ($y/H = 0.024$) and $y_0^+ = 311$ ($y/H = 0.307$) in the inner and outer layers are shown in Figure 10.a and b, respectively. The PDFs for water and the polymer solutions are symmetric around zero S_{11}, indicating that polymer chains are subjected to both stretching and compression. This is expected, as even in a uniaxial elongation, stretching occurs in the one direction whereas compression occurs in the other orthogonal directions. If the flow is under biaxial elongation, the fluid is expected to be simultaneously stretched in two directions and compressed in the third direction (squeezed). Therefore, the observed compression indicates stretching in another direction, which indicates local extensional viscosity in not isotropic. The relation of stretching and compression in orthogonal directions also means that characterizing S_{11} and S_{22} are sufficient as $S_{33} = -(S_{11}+S_{22})$.

At $y_0^+ = 24$ in Figure 10.a, the PDF of the S_{11} for polymeric flow become sharper and narrower with increase of polymer concentration. This means that the extensional viscosity of the polymer solution attenuated the streamwise strain-rate. The fluctuation range of S_{11} decreases from $\pm 800\ s^{-1}$ for water to $\pm 220\ s^{-1}$ at MDR, estimated using the width of the distribution at $1/e^2$ of the peak value. Further away from the wall at $y_0^+ = 311$ in Figure 10.b, the PDF profile of S_{11} for water is narrower with a larger peak compared with the PDF in the buffer layer, implying a smaller number of strong S_{11} fluctuations and large number of weak fluctuations. The effect of polymers on the PDF at $y_0^+ = 311$ is smaller compared with the PDFs at $y_0^+ = 24$.

(a) (b)

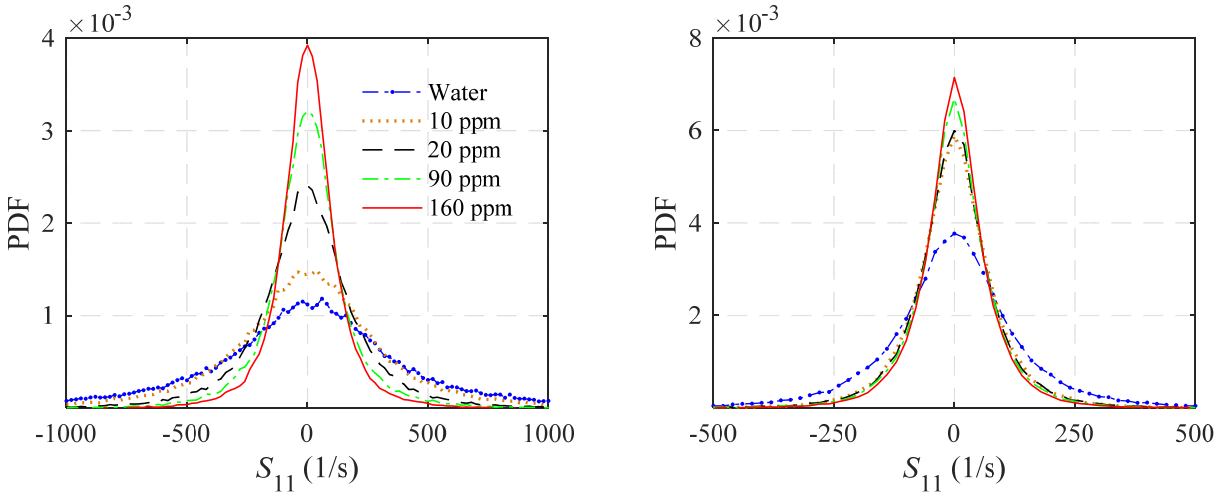

Figure 10. The PDF of S_{11} for the water and the four polymer cases at two wall-normal locations of (a) $y_0^+ = 24$ and (b) $y_0^+ = 311$.

The streamwise strain-rate distribution is used along with the relaxation time of each polymer solution to obtain the PDF of Weissenberg number, defined as $Wi_{11} = S_{11} \times \tau_{ext}$, in Figure 11. The PDF profiles of Wi_{11} at $y_0^+ = 24$ in Figure 11.a shows that the concentrated polymeric flows have lower probability of small Wi_{11} and higher probability of large Wi_{11} compared with dilute polymeric flows. The distribution of Wi_{11} for the 10 and 20 ppm approximately overlap while the PDF of Wi_{11} for 90 and 160 ppm are also close to each other. This overlap was not observed for PDF of S_{11} in Figure 10.a. Therefore, two distributions of Wi for low and high DR are suggested. The Wi_{11} decreases and the PDF shifts toward zero in the log layer as shown in Figure 11.b.

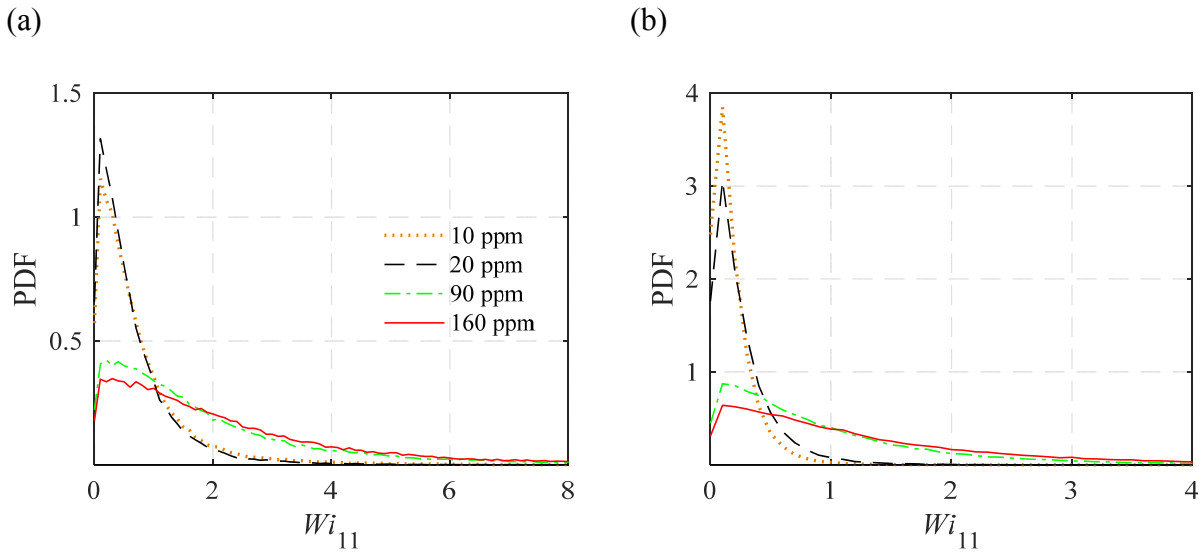

Figure 11. The PDF of Weissenberg number based on S_{11} at two wall-normal locations of (a) $y_0^+ = 24$ and (b) $y_0^+ = 311$.

The PDF profiles of S_{22} at the two wall-normal locations are shown in Figure 12.a and b. Similar to S_{11}, the distribution is symmetric and becomes narrower at higher DR with increase of extensional viscosity. In general, polymer chains are subject to smaller stretching and compression in the wall-normal direction than those observed in the streamwise direction. The PDF peak for water and the 10 ppm solution is higher at $y_0^+ = 311$ with respect to $y_0^+ = 24$, which shows a larger number of weak fluctuations away from the wall. The PDF of 160 ppm has higher peak in the buffer layer compared with those in the log layer while the PDF of 20 and 90 ppm have almost similar peaks at the two different wall-normal locations.

Figure 13.a and b show the variation of the PDFs of Wi_{22} *at* $y_0^+ = 24$ and $y_0^+ = 311$, respectively. Weissenberg number (Wi_{22}) is defined as the product of S_{22} and τ_{ext} here. The distribution of Wi_{22} in the buffer layer is similar as that in the log layer. The stretching of the polymers in streamwise direction is larger than the wall-normal direction since Wi_{22} reaches smaller values compared to Wi_{11} of Figure 11. It is also observed that the Wi_{22} distribution of low DR solutions (10 and 20 ppm) and the distribution of the high DR (90 and 160 ppm) overlap.

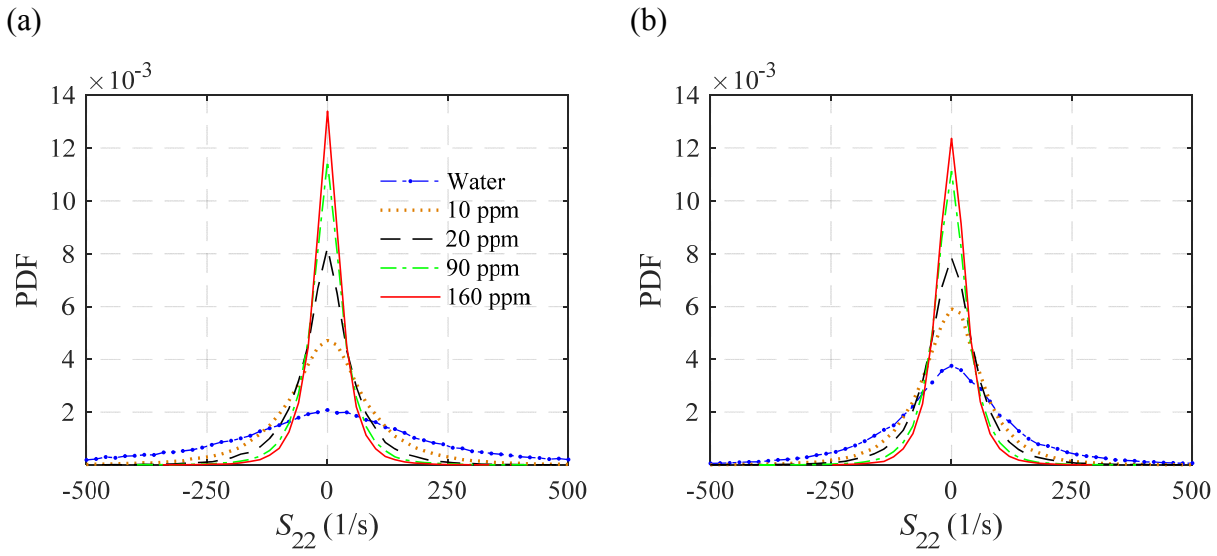

Figure 12. The PDF of wall-normal strain rate for water flow and the four polymer solutions at (a) y_0^+ = 24 and (b) y_0^+ = 311.

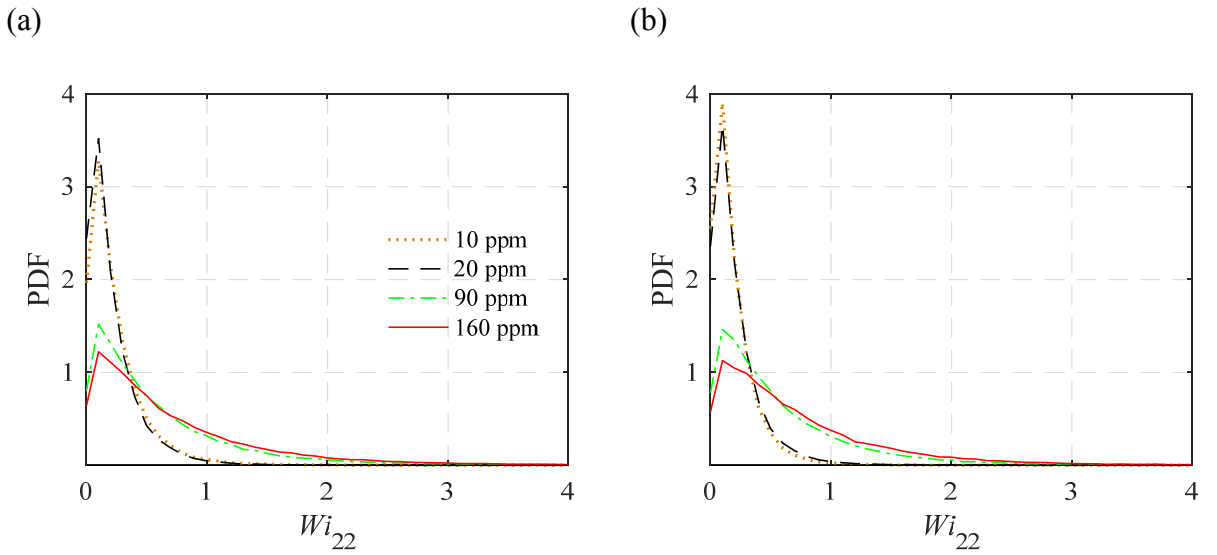

Figure 13. The PDF of Weissenberg number based on S_{22} at two wall-normal locations of (a) y_0^+ = 24 and (b) y_0^+ = 311.

3.3.3 Shear strain-rate

The shear strain-rate component of the velocity gradient tensor can indicate stretching of the polymer molecules due to shear and is calculated as

$$S_{12} = \left(\frac{\partial U}{\partial y} + \frac{\partial V}{\partial x}\right)/2 \tag{10}$$

The calculated S_{12} for water at $y_0^+ = 24$ has an asymmetric distribution skewed towards positive values in Figure 14.a. The peak of PDF for water is at ~300 1/s and is shifted to larger S_{12} of ~540 1/s for the 10 ppm solution. The shear strain rate for the 10 ppm solution has similar distribution to water while shifted to the right. However, the PDF peak for 20 ppm has moved towards a smaller peak value of 480 1/s, while the two concentrated polymeric flows have roughly similar peak location at 360 1/s. The distribution is narrower than water for the 20, 90, and 160 ppm. It is important to note that shear strain-rate for the polymeric flows has moved away from negative S_{12} region. Assuming that the $\partial U/\partial y$ is the dominant term of S_{12}, the lack of negative S_{12} means that $\partial U/\partial y$ is always positive in the polymeric solution. Therefore, local zones of low velocity, which are typically caused by ejection motions, do not exist in the polymer flows. This is consistent with attenuation of ejection events observed by Luchik and Tiederman (1988) and Walker and Tiederman (1990). Further away from the wall at $y_0^+ = 311$ in Figure 14.b, the PDF profile of polymeric solutions becomes narrow for all the solutions and the peak locations stays between 0 to 40 1/s with a relatively symmetric distribution.

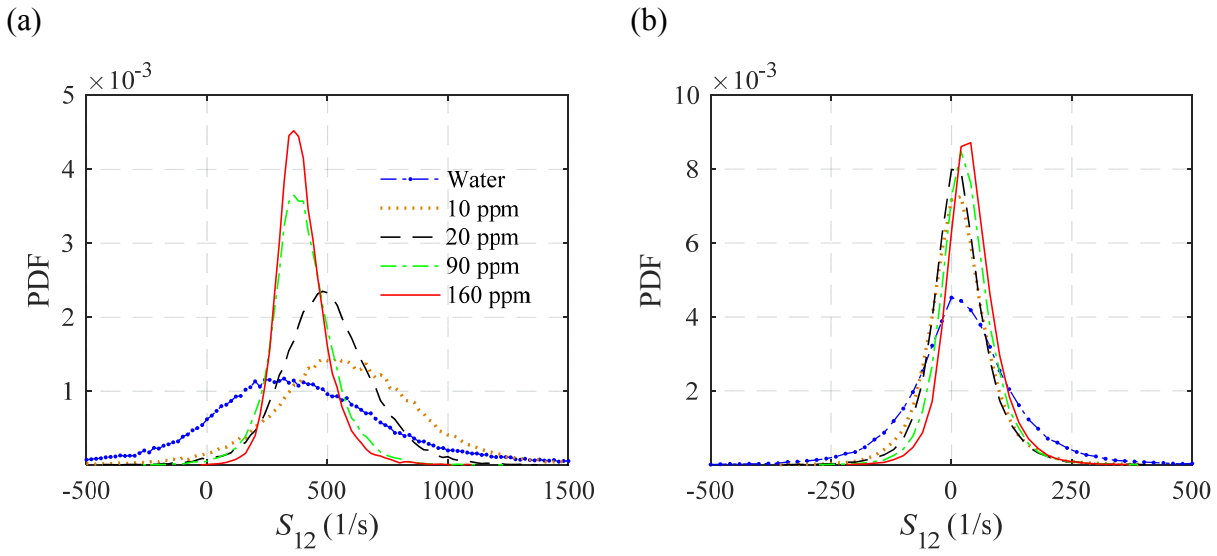

Figure 14. The PDF of shear rate for water and the four polymer solutions at two wall-normal locations of (a) $y_0^+ = 24$ and (b) $y_0^+ = 311$.

As it was discussed, in a turbulent flow shear and rotation occur at the same time, while the latter relaxes polymer stretching. If rotation is smaller than shear rate, the polymers are expected to significantly stretch. The balance of these two terms is evaluated here by calculating the absolute value of the ratio of instantaneous shear rate (S_{12}) to rotation (Ω_{12}), indicated as $R = S_{12}/\Omega_{12}$. The rotation term is also defined as

$$\Omega_{12} = \left(\frac{\partial U}{\partial y} - \frac{\partial V}{\partial x}\right)/2 \tag{11}$$

A large $|R|$ indicates higher shear rate with respect to rotation, and therefore stretching of the polymers. Figure 15.a shows the PDF of $|R|$ in the buffer layer at $y_0^+ = 24$. The PDF profile for water is relatively symmetric around $|R| = 1$ and covers a wide range of values from $|R| = 0.042$ to 1.67. However, all polymeric solutions have a narrower distribution of $|R|$ with almost equal rotation and shear rate (i.e., $|R| \sim 1$). In the log layer at $y_0^+ = 311$ in Figure 15.b, the PDF profile of R for water is highly asymmetric with a large probability of $|R| < 1$, which indicates stronger rotation. The polymeric solutions at 10 and 20 ppm do not have a significantly different PDF at this wall-normal location. At higher concentrations of 90 and 160 ppm, the PDF forms a strong peak at $|R| = 1$ with equivalent rotation and shear. Therefore, a balance of rotation and shear rate is observed in the buffer layer for all the solutions, while in the log layer it is only seen for the high DR cases. The polymers appear to be more effective in the buffer layer where shear rate is high. The need for

higher polymer concentration to affect the log layer is associated with the smaller shear with respect to rotation, which makes the polymer less effective.

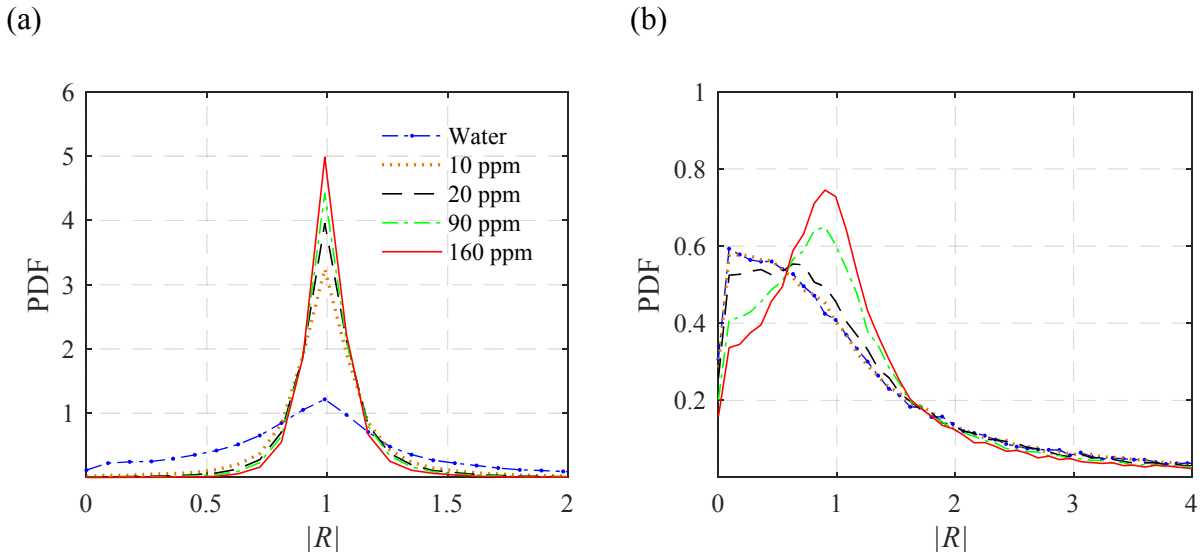

Figure 15. The PDF of absolute value of, $|R|$, for water and the four polymer solutions at (a) $y_0^+ = 24$ and (b) $y_0^+ = 311$.

The PDF profiles of Wi_{12} at $y_0^+ = 24$ and $y_0^+ = 311$ are shown in Figure 16.a and b, in which Wi_{12} is calculated as $Wi_{12} = S_{12} \times \tau_{ext}$. At $y_0^+ = 24$, the dilute polymer solutions show a narrow distribution of small Wi_{12} numbers while concentrated polymer solutions have a wide range of large Wi_{12} numbers. Small values of $Wi_{12} \leq 2$ are not present at MDR. In the log layer at $y_0^+ = 311$, shown in Figure 16.b, the magnitude of Wi_{12} is significantly smaller for the 10 and 20 ppm solutions.

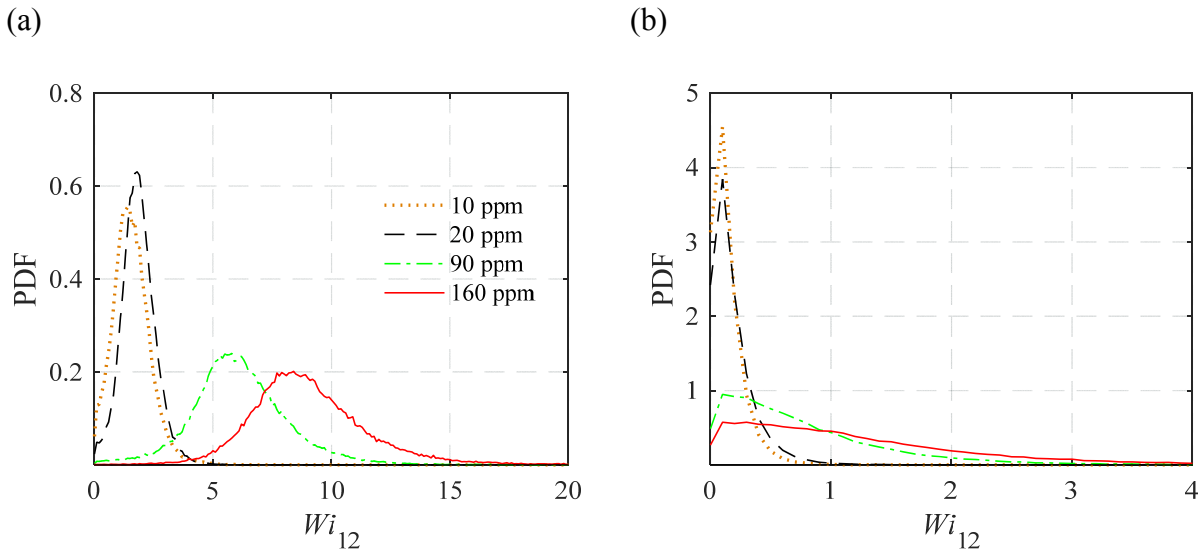

Figure 16. The PDF of Weissenberg number based on S_{12} at two wall-normal locations of (a) y_0^+ =24 and (b) y_0^+ =311.

3.4 Temporal scales of the flow

The power spectral density (PSD) of turbulence kinetic energy (K) for polymeric and water flows are compared at y_0^+ = 24 and y_0^+ = 311 in Figure 17.a and b, respectively. The PSD is computed using a Hanning window with resolution of 20 Hz, i.e. the width of one frequency bin. The effective noise bandwidth (ENBW) is 30 Hz. The K-spectra profiles at y_0^+ = 24 show that K decreases as polymer concentration increases, with the largest suppression at f >50 Hz. At low frequency of ~20 Hz, there is a smaller suppression of K for concentrated polymer solutions while the dilute polymeric flow at 10 ppm has a higher magnitude than water. Farther away from the wall at y_0^+ = 311, there is almost no reduction in energy at 20 Hz for all polymeric flows. The energy also remains constant for 90 and 160 ppm flows at frequencies between 500 and 2000 Hz. The suppression of K-spectra in the buffer layer is larger than that of log layer (y_0^+ = 311).

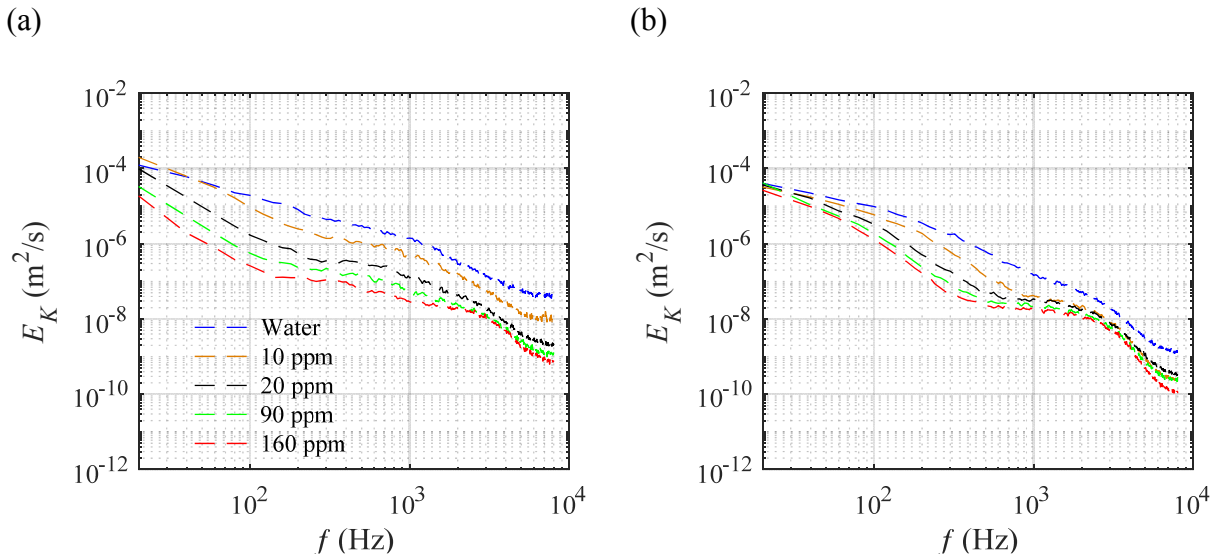

Figure 17. The PSD of the turbulence kinetic energy at (a) $y_0^+ = 24$ and (b) $y_0^+ = 311$.

4. Conclusion

An experimental investigation was carried out to characterize the rheology of polymeric solutions with 10, 20, 90, and 160 ppm polyacrylamide in terms of shear viscosity and extensional viscosity. Measurement of drag using pressure drop and velocity field using time-resolved planar particle image velocimetry (PIV) was also carried out in a turbulent channel flow at Reynold number of 20,000. The PIV measurements were used to investigate the effect of polymer rheology on mean velocity profile, Reynolds stresses, local strain rate and rotation, and spectral content of the flow.

The shear viscosity measurements showed that the dilute solutions with 10 and 20 ppm of polymer have a Newtonian behavior while the concentrated 90 and 160 ppm solutions have a shear thinning behavior. However, the maximum extensional viscosity and the relaxation time monotonously increased with increase of polymer concentration according to the capillary break-up extensional rheometer (CaBER). The relaxation time for the 160 ppm solution was 8.8 times larger than that of the 10 ppm solution. All the solutions showed strain hardening behavior while the concentrated solutions had larger magnitudes of strain and extensional viscosity. The filament drainage of concentrated polymer solution occurred at lower strain rate and higher extensional viscosity in comparison with the dilute solutions.

The 10, 20, 90, and 160 ppm solutions resulted in 25, 43, 51, and 57% drag reduction (DR) based on measurement of pressure drop. Although the difference in shear viscosity of 10 and 20

ppm is negligible, the DR of the 20 ppm polymeric flow was twice that of the 10 ppm solution. Therefore, the larger DR was associated with the larger relaxation time and extensional viscosity of the 20 ppm solution. The difference in DR of the 90 and 160 ppm is small although the relaxation time of the 160 ppm is about 30% larger. This suggests that increase of DR with relaxation time is not linear as DR approaches maximum drag reduction (MDR) with further increase of polymer concertation and relaxation time.

The mean velocity profiles of the 10 and 20 ppm concentration were close to the profile of turbulent flow of water due to negligible difference in their shear viscosity. The mean velocity profile of 90 and 160 ppm were located between profiles of turbulent and laminar flow of water. The velocity gradient at the wall was smaller for all polymeric flows. The results of DR from pressure drop agreed with DR estimation from PIV based on near-wall velocity gradient. The log-region was shifted upwards while it remained essentially parallel to water in Newtonian polymeric flows of 10 and 20 ppm. In the case of shear thinning 90 and 160 ppm solutions, the profiles in the log-layer were not only shifted upward but also had a higher slope than that of water. The peak value of streamwise Reynolds stress in the polymer flows were smaller and farther away from the wall relative to water. Reynolds shear stress and wall-normal Reynolds stress were close to zero at MDR. The viscous sublayer and buffer layer also thickened with increase of polymer concentration. Investigation of the quadrants of velocity fluctuations showed that the sweep and ejection events are significantly suppressed in polymeric flows, reflecting reduction of turbulence production.

Investigation of the spatial distribution of velocity gradient showed the extent of deformation of polymer molecules strongly depends on the wall-normal location. The PDF profiles of normal strain-rates had symmetrical distribution with respect to zero strain-rate due to both stretching and compression. Significant damping of normal and shear strain-rate fluctuations occurred in the buffer layer implying a larger extensional viscosity in this region. The attenuation of normal and shear strain-rates increased with increase in polymer concentration, and therefore extensional viscosity. The deformation of polymer molecules was mostly caused by streamwise and shear strain-rate. In the log-layer, polymer molecules did not significantly stretch since there were more flow instants with a strong local rotation compared with shear strain-rate. The probability profiles of shear strain-rate for polymeric flows were shifted toward positive values of strain-rate. At high polymer concentration, rotation and shear rate were balanced in both the buffer layer and log layer.

The distribution of Weissenberg number based on local strain-rate showed larger local *Wi* with increase of polymer concertation.

The power spectral density (PSD) of turbulence kinetic energy in the buffer layer showed that the 10 ppm solution was only able to damp the large eddies while the non-Newtonian polymeric flows showed a reduction over all frequencies. The suppression of the spectra was smaller in the log layer compared with buffer layer with the largest reduction at higher frequencies.

References

Anna, S. L., & McKinley, G. H. (2001). Elasto-capillary thinning and breakup of model elastic liquids. *Journal of Rheology*, *45*(1), 115-138.

Azad, M. S., Dalsania, Y., & Trivedi, J. J. (2018). Understanding the flow behaviour of copolymer and associative polymers in porous media using extensional viscosity characterization: Effect of hydrophobic association. *The Canadian Journal of Chemical Engineering*.

Berman, N. S. (1986). Velocity fluctuations in non-homogeneous drag reduction. *Chemical Engineering Communications*, *42*(1-3), 37-51.

Bhardwaj, A., Miller, E., & Rothstein, J. P. (2007). Filament stretching and capillary breakup extensional rheometry measurements of viscoelastic wormlike micelle solutions. *Journal of Rheology*, *51*(4), 693-719.

Bhardwaj, A., Richter, D., Chellamuthu, M., & Rothstein, J. P. (2007). The effect of pre-shear on the extensional rheology of wormlike micelle solutions. *Rheologica acta*, *46*(6), 861-875.

Burger, E. D., Munk, W. R., & Wahl, H. A. (1982). Flow increase in the Trans Alaska Pipeline through use of a polymeric drag-reducing additive. *Journal of Petroleum Technology*, *34*(02), 377-386.

Chhabra, R. P. (2010). Non-Newtonian fluids: an introduction. In *Rheology of complex fluids* (pp. 3-34). Springer, New York, NY.

Choi, K. S. (1989). Near-wall structure of a turbulent boundary layer with riblets. *Journal of fluid mechanics*, *208*, 417-458.

Christanti, Y., & Walker, L. M. (2001). Surface tension driven jet break up of strain-hardening polymer solutions. *Journal of Non-Newtonian Fluid Mechanics*, *100*(1-3), 9-26.

Clasen C, Plog JP, Kulicke WM, Owens M, Macosko C, Scriven LE, Verani M, McKinley GH. (2006). How dilute are dilute solutions in extensional flows?. *Journal of Rheology*, *50*(6), 849-881.

Delshad, M., Kim, D. H., Magbagbeola, O. A., Huh, C., Pope, G. A., & Tarahhom, F. (2008). Mechanistic interpretation and utilization of viscoelastic behavior of polymer solutions for improved polymer-flood efficiency. In *SPE Symposium on Improved Oil Recovery*. Society of Petroleum Engineers.

Donohue, G. L., Tiederman, W. G., & Reischman, M. M. (1972). Flow visualization of the near-wall region in a drag-reducing channel flow. *Journal of Fluid Mechanics*, *56*(3), 559-575.

Doyle, P. S., Shaqfeh, E. S., & Gast, A. P. (1997). Dynamic simulation of freely draining flexible polymers in steady linear flows. Journal of Fluid Mechanics, 334, 251-291.

Escudier, M. P., Nickson, A. K., & Poole, R. J. (2009). Turbulent flow of viscoelastic shear-thinning liquids through a rectangular duct: Quantification of turbulence anisotropy. *Journal of Non-Newtonian Fluid Mechanics*, *160*(1), 2-10.

Fabula, A. G. (1971). Fire-fighting benefits of polymeric friction reduction. *Journal of Basic Engineering*, *93*(3), 453-455.

Gampert, B., Braemer, T., Eich, T., & Dietmann, T. (2005). Rheo-optical investigations and near-wall turbulence structure of polymer solutions in turbulent channel flow. *Journal of non-newtonian fluid mechanics*, *126*(2-3), 115-121.

Ghaemi, S., Ragni, D., & Scarano, F. (2012). PIV-based pressure fluctuations in the turbulent boundary layer. *Experiments in fluids*, *53*(6), 1823-1840.

Harder, K. J., & Tiederman, W. G. (1991). Drag reduction and turbulent structure in two-dimensional channel flows. *Philosophical Transactions of the Royal Society of London A: Mathematical, Physical and Engineering Sciences*, *336*(1640), 19-34.

Hinch, E. J. (1977). Mechanical models of dilute polymer solutions in strong flows. *The Physics of Fluids*, *20*(10), S22-S30.

James, D. F., & Yogachandran, N. (2006). Filament-breaking length—a measure of elasticity in extension. *Rheologica acta*, *46*(2), 161-170.

Joseph DD (1990) Fluid dynamics of viscoelastic liquids. Springer, New York.

Kim, J., Moin, P., & Moser, R. (1987). Turbulence statistics in fully developed channel flow at low Reynolds number. *Journal of fluid mechanics*, *177*, 133-166.

Kim, N. J., Pipe, C. J., Ahn, K. H., Lee, S. J., & McKinley, G. H. (2010). Capillary breakup extensional rheometry of a wormlike micellar solution. *Korea-Australia Rheology Journal*, *22*(1), 31-41.

Lee, M., & Moser, R. D. (2015). Direct numerical simulation of turbulent channel flow up to $Re_\tau = 5200$. *Journal of Fluid Mechanics*, *774*, 395-415.

Luchik, T. S., & Tiederman, W. G. (1988). Turbulent structure in low-concentration drag-reducing channel flows. *Journal of Fluid Mechanics*, *190*, 241-263.

Lumley, J. L. (1969). Drag reduction by additives. *Annual review of fluid mechanics*, *1*(1), 367-384.

Lumley, J.L. (1973). Drag reduction in turbulent flow by polymer additives. *Macromolecular Reviews*, *1* **(**7), 263-290

Marshall, R. J., & Metzner, A. B. (1967). Flow of viscoelastic fluids through porous media. *Industrial & Engineering Chemistry Fundamentals*, *6*(3), 393-400.

McKinley, G. H. (2005). Visco-elasto-capillary thinning and break-up of complex fluids. Rheology Reviews; British Society of Rheology, (3) 1−48.

McKinley, G. H., & Sridhar, T. (2002). Filament-stretching rheometry of complex fluids. *Annual Review of Fluid Mechanics*, *34*(1), 375-415.

McKinley, G. H., & Tripathi, A. (2000). How to extract the Newtonian viscosity from capillary breakup measurements in a filament rheometer. *Journal of Rheology*, *44*(3), 653-670.

Meinhart, C. D., Wereley, S. T., & Santiago, J. G. (2000). A PIV algorithm for estimating time-averaged velocity fields. *Journal of Fluids Engineering*, *122*(2), 285-289.

Miller, E., Clasen, C., & Rothstein, J. P. (2009). The effect of step-stretch parameters on capillary breakup extensional rheology (CaBER) measurements. *Rheologica acta*, *48*(6), 625-639.

Min, T., Yoo, J. Y., Choi, H., & Joseph, D. D. (2003). Drag reduction by polymer additives in a turbulent channel flow. *Journal of Fluid Mechanics*, *486*, 213-238.

Mohammadtabar, M., Sanders, R. S., & Ghaemi, S. (2017). Turbulent structures of non-Newtonian solutions containing rigid polymers. *Physics of Fluids*, *29*(10), 103101.

Owolabi, B. E., Dennis, D. J., & Poole, R. J. (2017). Turbulent drag reduction by polymer additives in parallel-shear flows. *Journal of Fluid Mechanics*, *827*.

Plog, J. P., Kulicke, W. M., & Clasen, C. (2005). Influence of the molar mass distribution on the elongational behaviour of polymer solutions in capillary breakup. *Applied Rheology*, *15*(1), 28-37.

Ptasinski, P. K., Nieuwstadt, F. T. M., Van Den Brule, B. H. A. A., & Hulsen, M. A. (2001). Experiments in turbulent pipe flow with polymer additives at maximum drag reduction. *Flow, Turbulence and Combustion*, 66(2), 159-182.

Reichel, E. K., Voglhuber-Brunnmaier, T., Wolf, L., Beigelbeck, R., & Jakoby, B. (2016, October). Electric field driven extensional rheometry of synovial fluid. In *SENSORS, 2016 IEEE* (pp. 1-3). IEEE.

Renardy, M. (1995). A numerical study of the asymptotic evolution and breakup of Newtonian and viscoelastic jets. *Journal of non-newtonian fluid mechanics*, *59*(2-3), 267-282.

Rodd, L. E., Scott, T. P., Cooper-White, J. J., & McKinley, G. H. (2005). Capillary break-up rheometry of low-viscosity elastic fluids. *Applied Rheology, 15*(1), 12–27.

Rothstein, J. P. (2003). Transient extensional rheology of wormlike micelle solutions. *Journal of Rheology*, *47*(5), 1227-1247.

Rowin, W. A., Sanders, R. S., & Ghaemi, S. (2018). A Recipe for Optimum Mixing of Polymer Drag Reducers. *Journal of Fluids Engineering*, *140*(11), 111402.

Ryskin, G. (1987). Calculation of the effect of polymer additive in a converging flow. *Journal of Fluid Mechanics*, *178*, 423-440.

Ryskin, G. (1987). Turbulent drag reduction by polymers: a quantitative theory. *Physical review letters*, *59*(18), 2059.

Schümmer, P., & Tebel, K. H. (1983). A new elongational rheometer for polymer solutions. *Journal of Non-Newtonian Fluid Mechanics*, *12*(3), 331-347.

Sellin, R. H. J. (1978). Drag reduction in sewers: first results from a permanent installation. *Journal of Hydraulic Research*, *16*(4), 357-371.

Smith, D. E., Babcock, H. P., & Chu, S. (1999). Single-polymer dynamics in steady shear flow. *Science*, *283*(5408), 1724-1727.

Stelter, M., & Brenn, G. (2002). Elongational rheometry for the characterization of viscoelastic liquids. Chemical engineering & technology, 25(1), 30-35.

Taylor, G. I. (1923). Stability of a viscous liquid contained between two rotating cylinders. Philosophical Transactions of the Royal Society of London. Series A, Containing Papers of a Mathematical or Physical Character, 223, 289-343.

Theunissen, R., Scarano, F., & Riethmuller, M. L. (2008). On improvement of PIV image interrogation near stationary interfaces. *Experiments in Fluids*, *45*(4), 557-572.

Tiederman, W. G., Luchik, T. S., & Bogard, D. G. (1985). Wall-layer structure and drag reduction. *Journal of Fluid Mechanics*, *156*, 419-437.

Toms, B. A. (1948). Some observations on the flow of linear polymer solutions through straight tubes at large Reynolds numbers. *Proc. of In. Cong. On Rheology,* 135-141.

Virk, P. S. (1975). Drag reduction fundamentals. *AIChE Journal*, *21*(4), 625-656.

Virk, P. S., Merrill, E. W., Mickley, H. S., Smith, K. A., & Mollo-Christensen, E. L. (1967). The Toms phenomenon: turbulent pipe flow of dilute polymer solutions. *Journal of Fluid Mechanics*, *30*(2), 305-328.

Virk, P. S., Mickley, H. S., & Smith, K. A. (1970). The ultimate asymptote and mean flow structure in Toms' phenomenon. *Journal of applied Mechanics*, *37*(2), 488-493.

Walker, D. T., & Tiederman, W. G. (1990). Turbulent structure in a channel flow with polymer injection at the wall. *Journal of Fluid Mechanics*, *218*, 377-403.

Warholic, M. D., Heist, D. K., Katcher, M., & Hanratty, T. J. (2001). A study with particle-image velocimetry of the influence of drag-reducing polymers on the structure of turbulence. *Experiments in fluids*, *31*(5), 474-483.

Warholic, M. D., Massah, H., & Hanratty, T. J. (1999). Influence of drag-reducing polymers on turbulence: effects of Reynolds number, concentration and mixing. *Experiments in fluids*, *27*(5), 461-472.

Wei, T., & Willmarth, W. W. (1992). Modifying turbulent structure with drag-reducing polymer additives in turbulent channel flows. *Journal of Fluid Mechanics*, *245*, 619-641.

White, C. M., Somandepalli, V. S. R., & Mungal, M. G. (2004). The turbulence structure of drag-reduced boundary layer flow. *Experiments in fluids*, 36(1), 62-69

Willmarth, W. W., & Lu, S. S. (1972). Structure of the Reynolds stress near the wall. *Journal of Fluid Mechanics*, *55*(1), 65-92.

Yarin, A. L. (1993). *Free liquid jets and films: hydrodynamics and rheology*. Longman, Harlow and Wiley, New York.